Journal of Alloys and Compounds 823 (2020) 153770

Contents lists available at ScienceDirect

Journal of Alloys and Compounds

journal homepage: http://www.elsevier.com/locate/jalcom

Mn_2FeSi: An antiferromagnetic inverse-Heusler alloy

Anil Aryal [a], Said Bakkar [a], Hassana Samassekou [a], Sudip Pandey [a], Igor Dubenko [a], Shane Stadler [b], Naushad Ali [a], Dipanjan Mazumdar [a, *]

[a] Physics Department, Southern Illinois University Carbondale, IL, 62901, USA
[b] Department of Physics and Astronomy, Louisiana State University, Baton Rouge, LA, 70803, USA

ARTICLE INFO

Article history:
Received 11 October 2019
Received in revised form
18 December 2019
Accepted 8 January 2020
Available online 13 January 2020

Keywords:
Heusler alloys
Magnetic materials
Spintronics
Intermetallics

ABSTRACT

Search for low-moment magnetic materials with high spin-polarization is important for emerging spintronics applications. In this work, we have conducted detailed growth and characterization along with complementary first-principles calculations to investigate the structure and magnetism of Mn_2FeSi, which is a prospective inverse-Heusler material. We confirm that Mn_2FeSi adopts a cubic inverse-Heusler structure, in excellent agreement with theory. The magnetic and resistivity measurements show an antiferromagnetic behavior with a Néel temperature of 48 K, which is consistent with prior experimental reports. We find that a low-moment state with higher ordering temperature (150–200 K) can be stabilized under certain growth conditions. Supporting calculations show that Neel-type antiferromagnetic states are energetically very close to the ferrimagnetic ground state. Our work provides evidence that Mn_2FeSi may be interesting for exploring newer applications with low-moment materials, but the ordering temperatures are low for viable practical applications.

1. Introduction

The search for new magnetic materials for next-generation spintronics applications is a very important area of research. Heusler alloys are particularly interesting as they can support, in theory, 100% spin polarization which is highly desired in spintronics devices that utilize the giant and tunnel magnetoresistance effect. It is also recognized for sometime that spintronic devices can be applied to memory technologies by incorporating the experimentally-proven spin-transfer torque (STT) effect [1–3]. Applications in such areas dictate a broader set of properties in the active magnetic material such as perpendicular magnetic anisotropy (PMA) [4], low magnetization and damping [5,6] apart from high spin-polarization. Realizing such properties in the bulk form is challenging and motivated a number of theory-driven searches [7–9] within the Heulser family [10]. Tetragonal materials that promote high bulk PMA can suffer from low spin-polarization [8,9,11,12] and low tunnel magnetoresistance [13–15], whereas cubic systems with potentially nearly 100% spin-polarization [7] do not support PMA. It is therefore quite topical to explore and expand the experimental search to other prospective candidates, including antiferromagnets [16].

Inverse-Heuslers (general formula X_2YZ) are emerging as a promising sub-family in the search for low-moment systems required for STT applications [10]. Encouragingly, recent first principles theory calculations have identified several families supporting low magnetization [7–9], particularly the Mn_2FeZ family (Z = Al, Ge, Si, In, Ga). Therefore, there is a renewed interest in investigating such systems. The structure and magnetic properties of some of these materials have been reported. Mn_2FeGa is reported to stabilize in a tetragonal structure [9], while Mn_2FeAl adopts a non-Heusler cubic structure [17]. There are some existing experimental reports on Mn_2FeSi, mainly as part of the $Fe_{3-x}Mn_xSi$ family. Leitao et al. [18] report an antiferrmagnetic to paramagnetic transition at 50 K with an $L2_1$ structure. Miki et al. [19] and Yoon et al. [20] also report an AFM-PM transition at 50 K with a lattice constant of 5.68 Å from neutron diffraction measurements. Some groups have investigated $Fe_{3-x}Mn_xSi$ ($1 \leq x < 2$) [21–23] and off-stoichiometric $Mn_{48}Fe_{34}Si_{18}$ [24].

In this work, a detailed experimental characterization of Mn_2FeSi is reported motivated by prior theoretical investigations that identified Mn_2FeSi as a ferrimagnetic inverse-Heusler material [7,9,25]. The major experimental conclusion of this work is that Mn_2FeSi is an antiferromagnetic inverse-Hesuler material. Our study agrees with prior experimental reports on the magnetic

* Corresponding author.
E-mail address: dmazumdar@siu.edu (D. Mazumdar).

https://doi.org/10.1016/j.jallcom.2020.153770
0925-8388/

behavior of Mn_2FeSi [18–20], but we additionally confirm the theoretical prediction that Mn_2FeSi stabilizes in the inverse-Heusler and not the full-Heusler phase. Additionally, quenched bulk and thin film samples of Mn_2FeSi are observed to stabilize in a low-moment state with a high Curie temperature. Supporting first-principles calculations show that antiferromagnetic states are practically degenerate in energy compared to the ferrimagnetic ground state. Our work provides evidence that Mn_2FeSi can serve as a prototype inverse-Heusler antiferromagnet and such materials may be useful in exploring emerging applications in the area of spintronics. In principle, this study could be extended to other unexplored members of the Mn_2FeZ family (Z = Ge, In, for example). However, we found that it is difficult to stabilize nearly pure cubic phases of these materials using arc-melting method. Therefore, we focused on Mn_2FeSi in this study.

2. Experiment

Approximately 4 g of bulk polycrystalline Mn_2FeSi compound was prepared by conventional arc-melting 99.99% pure elements in an ultra-high purity argon atmosphere. The sample was flipped and re-melted multiple times to ensure homogeneity. The final as-melted ingot was cut into two halves using a slow moving diamond wheel cutter. The first half of the sample was further cut into small pieces. Pieces of the sample were then wrapped in tantalum foil and annealed in high vacuum ($\sim 10^{-6}$ Torr) for 2–10 days at temperatures ranging from 500 °C to 800 °C. Only the 500 °C data is shown here since it produced the best and nearly pure phase X-ray diffraction pattern. The second half of the ingot was remelted and quenched immediately by dropping in cold water. Both as-quenched and annealed samples are discussed in details. Supporting thin-film growth was accomplished using a combination of d.c and r.f magnetron sputtering with co-sputtered elemental Mn, Fe and Si targets in a high vacuum chamber with a base pressure better than 4×10^{-9} Torr. Film thickness was verified using X-ray reflectivity technique. The microstructure and the chemical composition of the samples were verified using the FEI Quanta FEG 450 SEM equipped with EDS detectors. The phase purity and crystal structure were studied by powder X-Ray diffraction (XRD) using Rigaku SmartLab diffractometer (CuK_α radiation) at room temperature. Rietveld refinement of the XRD pattern was carried out using the MATCH software based on FULLPROF software [26]. XPS analysis was not conducted as it was difficult to cleave or polish the hard samples *in-situ* under high vacuum which is necessary to remove the oxidized surface. The magnetization measurements were performed using a superconducting quantum interference device (SQUID by Quantum Design) magnetometer in the temperature range 5–380 K in a magnetic field up to 5 T. Magnetization measurements were taken following the zero-field cooling (ZFC), field-cooling (FC) and field-cooled-heating (FCH) protocols. The electrical resistivity was measured by four-probe method in the temperature interval of 5–380 K. Resistivity measurements were performed only on the annealed samples and not on the quenched samples as they were brittle and harder to cut into proper shapes. First-principles calculations was carried out using density-functional theory as implemented in the WIEN2K package [27] employing the PBE-GGA exchange correlation potential. Magnetic calculations were performed on an 8-atom tetragonal unit cell incorporating AFM ordering [28]. The energy convergence of 7×10^{-6} Ry (less than 0.1 meV), and RMT values of 1.94 for Si and 2.28 for Mn and Fe were chosen. A $19 \times 19 \times 13$ k-point grid was employed for both FM and AFM calculations with 700 nonequivalent points.

3. Results and discussions

3.1. Micro and crystal structure of Mn_2FeSi

Structurally, the inverse-Heusler structure (XA, Hg_2CuTi type) can be obtained from the full-Heusler ($L2_1$, Cu_2MnAl type) by switching one of the X atoms with a Y atom. The Z and Y elements are located at the (0, 0, 0) and $(\frac{1}{4}, \frac{1}{4}, \frac{1}{4})$ respectively in Wyckoff coordinates, while the X elements are at $(\frac{3}{4}, \frac{3}{4}, \frac{3}{4})$ and $(\frac{1}{2}, \frac{1}{2}, \frac{1}{2})$ position. First-principles calculations have highlighted several cubic and tetragonal Manganese-based inverse-Heuslers with desirable properties [7–9,25,29–31].

The SEM micrographs of annealed and as-quenched bulk samples are shown in gray color in Fig. 1. The fractured surface of annealed samples (top panel) showed a homogeneous single composition phase with no visible secondary phase. The metallographic optical image of annealed Mn_2FeSi (inset of Fig. 1 (a)) also show large grains without voids that indicates the formation of a homogeneous crystal structure. The SEM micrographs of as-quenched Mn_2FeSi (bottom panel, Fig. c and d), on the other hand, show a granular and porous microstructure. Interestingly, the formation of microscopic domains inside the grains are observed (Fig. 1 (d)).

In Fig. 2, the XRD pattern of the (a) as-cast (b) as-quenched and (c) 500 °C - 10 days annealed Mn_2FeSi are shown along with their Reitveld fits. The common Heusler diffraction peaks are clearly identified, even for the as-cast sample, that confirms the cubic nature of the material. The fitted lattice parameter is close to 5.68 Å which is only about 1.4% higher than the theoretical estimate of 5.60 Å [7,9,25], and in excellent agreement with prior experimental reports [19,20]. The XRD peak positions of the three samples are tabulated in Table T1 of supplementary material. A small impurity peak was observed in all samples close to 43.4° (indicated by *) which could not be assigned to any Heusler diffraction peak. The diffraction patterns obtained for samples annealed for different times at 500 °C is shown in Fig. S1. The relative intensity of the (111)

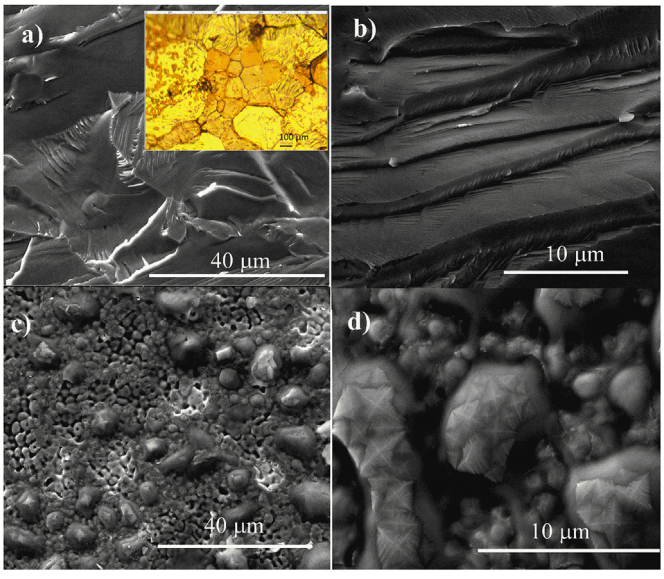

Fig. 1. SEM image of annealed (top panel) and as-quenched (bottom panel) Mn_2FeSi at different magnifications. Inset of (a) Metallographic image of a bulk Mn_2FeSi sample annealed at 500C for 48 h obtained by etching the sample with a marble etchant showing clear crystallographic grains.

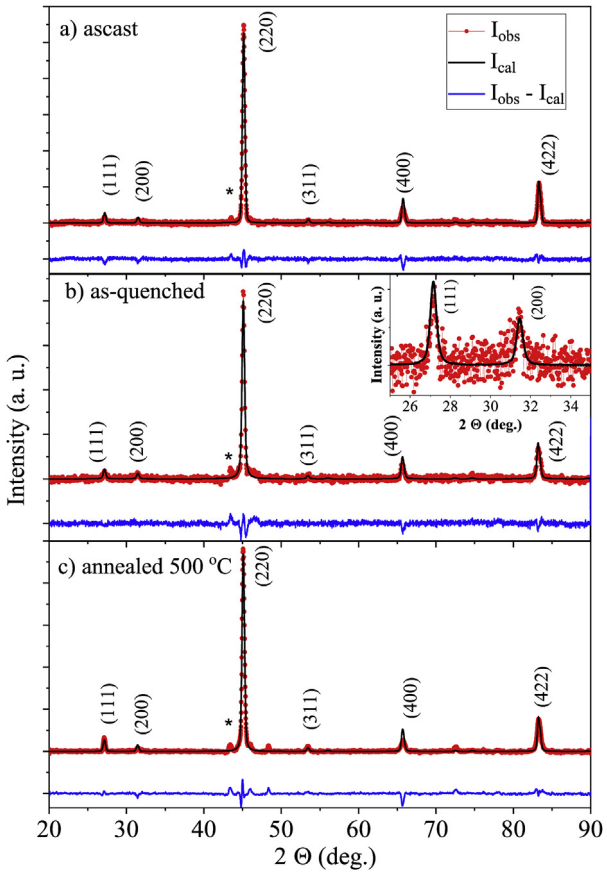

Fig. 2. Room temperature XRD pattern of (a) as-cast (b) as-quenched and (c) annealed samples and their Reitveld fitting. Inset of (b): Enlarged view of the XRD patterns of as-quenched sample in the 2θ range from 25 to 35 deg showing the (111) and (200) peaks.

peak, in particular, increases significantly after prolonged annealing that is attributed to the enhancement of the inverse-Heusler order.

Precise structural order evaluation based on a casual inspection of X-ray diffraction is difficult as the full ($L2_1$) and inverse-Heusler (XA) structures are almost identical with only varying relative intensity of the (111) and (200) superlattice peaks compared to the (220) peak. The Reitveld analysis confirmed the inverse-Heusler (XA) nature of Mn_2FeSi as the $L2_1$ structure produced a much inferior agreement. Specifically, the relative intensity of the (111) peak is higher than the (200) peak for the inverseHeusler structure (as shown in the inset of Fig. 2(b) and in Fig. S1). The simulated trend is opposite for the $L2_1$ structure i.e, (200) peak has a higher relative intensity than (111), which disagrees with our experimental data. We thereby conclusively confirm the theoretical prediction that Mn_2FeSi stabilizes in an inverse-Heusler structure.

3.2. Magnetic measurements and supporting first-principle calculations

Typically, almost all Mn-based inverse-Heuslers are predicted to be ferrimagnetic in the ground state with unequal anti-parallel moments at the two Mn sites whereas the magnetic moment on the second magnetic atom (Fe in the case of Mn_2FeSi) is significantly smaller and parallel to the nearest-neighbor Mn atom occupying the $(\frac{1}{2}, \frac{1}{2}, \frac{1}{2})$ position. The magnetic moment values are practically identical in both $L2_1$ and *XA* structures, and, therefore, it is hard to distinguish the crystal structure from magnetic measurements.

The detailed site-specific moment values obtained for an 8-atom Mn_2FeSi supercell are shown in Table T2 of the supplementary material. The values are in good agreement with literature reports [7]. Calculations on the 8-atom antiferromagnetic supercell show that the magnetic moment at the Fe and the $(\frac{1}{4}, \frac{1}{4}, \frac{1}{4})$ Mn site is practically zero while the moment at the $(\frac{1}{2}, \frac{1}{2}, \frac{1}{2})$ Mn site is compensated. Energetically, the perfectly compensated AFM ordering is only 4 meV larger than the ferrimagnetic ground state (see Table T2 and Fig. S5). This indicates that both solutions are practically degenerate. Our experimental results are consistent with compensated (antiferromagnetic) moments as explained below.

The isofield M(T) curves on heating and cooling in the applied magnetic field of H = 100 Oe for annealed (500 °C - 2 days) and as-quenched samples is shown in Fig. 3 (a) and (b). A cusp-like behavior in the M(T) curve was observed at low temperatures indicating an antiferromagnetic ordering in the annealed Mn_2FeSi alloy. The magnetization increased rapidly at low temperatures, peaking at ~ 48 K that corresponds to the Néel temperature (T_N) and decreased gradually above T_N on heating. This value compares very favorably with the available reports [18–20]. It is known that the magnetic susceptibility (χ) follows the Curie-Weiss law in the paramagnetic phase given by, $\chi = \frac{C}{T-\theta_P}$ where, C is the Curie Constant and θ_P is the Curie-Weiss temperature. The value of θ_P was obtained from the linear fit of the temperature dependence of the inverse susceptibility χ^{-1}(T) curve in the paramagnetic region (see Fig. S2). The negative value of θ_P (~ - 34 K) confirms the antiferromagnetic ordering of the spins in the Mn_2FeSi alloy. As shown in the inset of Fig. 3(a), the field dependence of magnetization M(H) at temperatures below and above T_N is linear, a behavior typical of antiferromagnetic and paramagnetic materials.

A number of interesting features are also observed in the

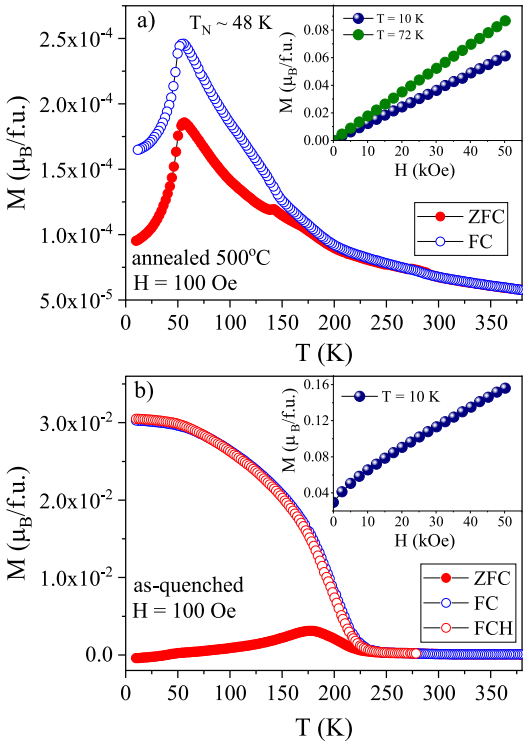

Fig. 3. Temperature dependence of Magnetization M(T) curves of (a) annealed (500 °C for 2 days) and (b) as-quenched Mn_2FeSi during heating and cooling process at applied field of 100 Oe. Inset of Fig (a) and (b) show the M(H) curves for annealed and as-quenched samples respectively.

magnetization data. First, a bifurcation of the field-cooled and the zero field-cooled data is noticed. It is hypothesized that it may due to the existence of uncompensated spins/domains at the surface of the sample that align with the external magnetic field at low temperatures when thermal fluctuations are quenched. The residual moment could be stabilized due to defect-induced domain wall pinning. Secondly, a small peak in the ZFC curve at around 150 K is observed that is attributed to inhomogeneity in the sample. This can be concluded because the peak is greatly reduced when the sample is annealed for 10 days (see supplementary data, Fig. S3). Additionally, it is concluded from this data that the dominant magnetic behavior of annealed samples are not sensitive to the annealing time as the M(T) curve of the sample annealed for 10 days @ 500 °C shows a near identical behavior to the 48-hr annealed sample (Fig. 3(a)). Therefore, the appearance of stronger impurity peaks after prolonged annealing has minimal bearing on the antiferromagnetic character of Mn_2FeSi. This reaffirms that antiferromagnetism is intrinsic to the Heusler phase. It is worth mentioning that the 48 K antiferromagnetic transition temperature is reasonably close to the 71 K theoretical estimate for the ferrimagnetic state [32]. Therefore, overall, the most significant theory-experiment disagreement is regarding the value of the magnetic moment. While calculations do not completely resolve the theory-experiment discrepancy, it is satisfactory to find that the compensated states are practically degenerate to the ferrimagnetic ground state and may explain why they can be stabilized at high growth temperatures. Additional temperature dependent calculations might perhaps shed further light, but was beyond the scope of this work.

In contrast to the annealed sample, the M(T) curves of the as-quenched Mn_2FeSi shows a ferrimagnetic behavior at H = 100 Oe with critical temperature (T_C) of ~ 200 K as shown in Fig. 3(b). A small curvature and non-saturating behavior of the M(H) curves at T = 10 K was observed (see inset of Fig. 3(b)). The non-linearity in M(H) curve at low field indicates that the magnetic moments are not fully compensated in the quenched sample. However, the estimated magnetic moment value is roughly two-orders of magnitude smaller than first-principles estimates for the ferrimagnetic state.

Additional synthesis of stiochiometric Mn_2FeSi thin-films was performed on (001)-oriented MgO substrates at 600 °C to investigate whether the 2 μ_B/f.u ferrimagnetic state can be epitaxially stabilized. The magnetic behavior is shown in Fig. S4. The behavior is strikingly similar to quenched bulk samples apart from the uptick in the magnetization value below 20 K that is attributed to paramagnetic defects within the MgO substrate from induced oxygen vacancies due to the high temperature deposition process [33]. The magnetic moment value, though higher than quenched samples, is still only a fraction of the theoretical estimate for the ferrimagnetic state. So taking all magnetic data together, it is concluded that magnetically Mn_2FeSi shows a compensated behavior, in agreement with prior experimental reports [18–20]. Interestingly, such theory-experiment discrepancy is also reported for Mn_3Si [8].

3.3. Electrical resistivity measurements

Resistivity measurements also support the presence of a strong antiferromagnetic transition at 47-48 K. In Fig. 4, the temperature dependence of resistivity $\rho(T)$ of the optimally annealed sample is shown at zero magnetic field. Mn_2FeSi shows a typical metallic behavior with large residual resistivity (ρ_o) = 324 $\mu\Omega cm$ at T = 5 K and residual resistivity ratio ($\frac{\rho_{300K}}{\rho_{5K}}$) of about 1.3. A saturation of resistivity at higher temperatures in the $\rho(T)$ curve was observed that is uncommon for metallic systems. At low temperatures (T < T_N), the resistivity decreases rapidly which can be attributed to the onset of magnetic ordering. Further evidence to this effect is obtained in the $\frac{d\rho}{dT}$ vs T curve as shown in the inset (a) of Fig. 4. The clear maxima at 47–48 K matches well with the value of T_N obtained from M(T) measurement (Fig. 3(a)). Therefore, it is clear that the resistivity behavior is also consistent with the observed magnetic transition.

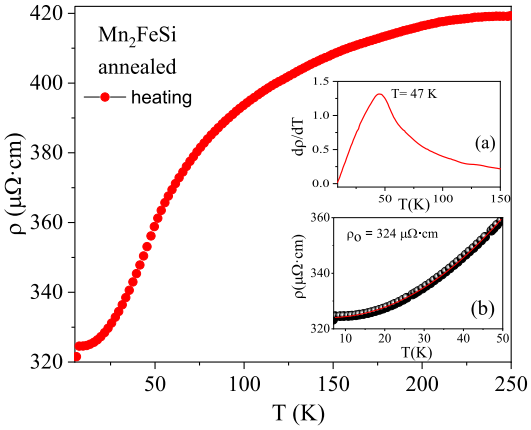

Fig. 4. Temperature dependence of Resistivity of optimally annealed Mn_2FeSi. Inset: (a) $\frac{d\rho}{dT}$ vs T curve (b) T^2 dependence of resistivity at low temperatures.

The temperature dependence of resistivity in magnetic materials is usually interpreted using the Matthiessen's rule given by,

$$\rho(T) = \rho_o + \rho_{e-ph}(T) + \rho_{e-mag}(T)$$

where, $\rho(T)$ is the total resistivity, ρ_o is the residual resistivity, $\rho_{e-ph}(T)$ is the resistivity due to electron-phonon scattering (with linear dependence in T) and $\rho_{e-mag}(T)$ is the resistivity due to electron-magnon scattering (with T^2 dependence).

$$\rho(T) = \rho_o + AT + BT^2,$$

where A and B are constants.

As shown in the inset (b) of Fig. 4, the resistivity of Mn_2FeSi follow a T^2 law at low temperatures (T < T_N) which indicates that magnetic scattering is dominant at low temperatures. However at high temperatures, the resistivity of Mn_2FeSi deviates from the Matthiessen's rule showing a saturation in resistivity. Such a saturation tendency at higher temperatures has been previously reported in other magnetic materials and explained on the basis of Ioffe-Regel criterion [34] which is satisfied when the mean free path approaches interatomic distances. Additionally, spin-lattice disorder can be also important [35,36].

4. Conclusion

In conclusion, the crystal structure and magnetic behavior of Mn_2FeSi are investigated thoroughly. We find that the experimental crystal structure agrees very well with the predicted inverse-Heusler ordering, while we confirm the antiferromagnetic behavior as reported in the literature. A low-moment state with a reasonably high Curie temperature is stabilized in quenched bulk and thin-film samples. First-principles calculations support the possibility of compensated magnetic states, as observed in our experiments.

Declaration of competing interests

The authors declare that they have no known competing

financial interests or personal relationships that could have appeared to influence the work reported in this paper.

CRediT authorship contribution statement

Anil Aryal: Data curation, Formal analysis, Investigation, Writing - original draft, Validation, Visualization. **Said Bakkar:** Investigation. **Hassana Samassekou:** Investigation. **Sudip Pandey:** Investigation. **Igor Dubenko:** Supervision, Methodology. **Shane Stadler:** Funding acquisition, Supervision. **Naushad Ali:** Funding acquisition, Supervision. **Dipanjan Mazumdar:** Funding acquisition, Methodology, Conceptualization, Supervision, Project administration, Formal analysis, Writing - review & editing.

Acknowledgments

DM would like to acknowledge NSF CAREER grant (ECCS 1846829) and NSF DMREF grant No. 1235396 for support of this work. NA and SS acknowledge the support received from U. S. Department of Energy (DOE), Office of Science, Basic Energy Sciences (BES) under Award No. DE-FG02-06ER46291 (SIU) and DE-FG02-13ER46946 (LSU). DM would also like to thank Jianhua Ma and Bill Butler for numerous discussions on inverse-Heuslers. This work used the Extreme Science and Engineering Discovery Environment (XSEDE) which is supported by National Science Foundation grant number ACI-1548562. Computational resources were provided at the San Diego Supercomputer Center (comet) through allocation DMR160135.

Appendix A. Supplementary data

Supplementary data to this article can be found online at https://doi.org/10.1016/j.jallcom.2020.153770.

References

[1] J.C. Slonczewski, Current-driven excitation of magnetic multilayers, J. Magn. Magn. Mater. 159 (1996). L1–L7.
[2] L. Berger, Emission of spin waves by a magnetic multilayer traversed by a current, Phys. Rev. B 54 (1996) 9353.
[3] J. Katine, F. Albert, R. Buhrman, E. Myers, D. Ralph, Current-driven magnetization reversal and spin-wave excitations in Co/Cu/Co pillars, Phys. Rev. Lett. 84 (2000) 3149.
[4] S. Ikeda, K. Miura, H. Yamamoto, K. Mizunuma, H.D. Gan, M. Endo, S. Kanai, J. Hayakawa, F. Matsukura, H. Ohno, A perpendicular-anisotropy CoFeB-MgO magnetic tunnel junction, Nat. Mater. 9 (2010) 721.
[5] J. Zhang, T. Phung, A. Pushp, Y. Ferrante, J. Jeong, C. Rettner, B.P. Hughes, S.-H. Yang, Y. Jiang, S. Parkin, Bias dependence of spin transfer torque in Co_2MnSi Heusler alloy based magnetic tunnel junctions, Appl. Phys. Lett. 110 (2017) 172403.
[6] B. Dieny, M. Chshiev, Perpendicular magnetic anisotropy at transition metal/oxide interfaces and applications, Rev. Mod. Phys. 89 (2017), 025008.
[7] J. Ma, J. He, D. Mazumdar, K. Munira, S. Keshavarz, T. Lovorn, C. Wolverton, A.W. Ghosh, W.H. Butler, Computational investigation of inverse Heusler compounds for spintronics applications, Phys. Rev. B 98 (2018), 094410.
[8] S.V. Faleev, Y. Ferrante, J. Jeong, M.G. Samant, B. Jones, S.S.P. Parkin, Heusler compounds with perpendicular magnetic anisotropy and large tunneling magnetoresistance, Phys. Rev. Mater. 1 (2017), 024402.
[9] S.V. Faleev, Y. Ferrante, J. Jeong, M.G. Samant, B. Jones, S.S.P. Parkin, Origin of the tetragonal ground state of Heusler compounds, Phys. Rev. Appl. 7 (2017), 034022.
[10] C. Felser, L. Wollmann, S. Chadov, G.H. Fecher, S.S.P. Parkin, Basics and prospective of magnetic Heusler compounds, Apl. Mater. 3 (2015), 041518.
[11] B. Balke, G. Fecher, J. Winterlik, C. Felser, Mn_3Ga, a compensated ferrimagnet with high Curie temperature and low magnetic moment for spin torque transfer applications, Appl. Phys. Lett. 90 (2007) 152504.
[12] H. Kurt, K. Rode, M. Venkatesan, P. Stamenov, J.M.D. Coey, High spin polarization in epitaxial films of ferrimagnetic Mn_3Ga, Phys. Rev. B 83 (2011), 020405(R).
[13] J. Jeong, Y. Ferrante, S.V. Faleev, M.G. Samant, C. Felser, S.S.P. Parkin, Termination layer compensated tunnelling magnetoresistance in ferrimagnetic Heusler compounds with high perpendicular magnetic anisotropy, Nat. Commun. 7 (2016), 10276.
[14] T. Kubota, Y. Miura, D. Watanabe, S. Mizukami, F. Wu, H. Naganuma, X. Zhang, M. Oogane, M. Shirai, Y. Ando, Magnetoresistance effect in tunnel junctions with perpendicularly magnetized DO_{22}-$Mn_{3-\delta}Ga$ electrode and MgO barrier, Appl. Phys. Exp. 4 (2011), 043002.
[15] K.Z. Suzuki, R. Ranjbar, J. Okabayashi, Y. Miura, A. Sugihara, H. Tsuchiura, S. Mizukami, Perpendicular magnetic tunnel junction with a strained Mn-based nanolayer, Sci. Rep. 6 (2016), 30249.
[16] T. Jungwirth, J. Sinova, A. Manchon, X. Marti, J. Wunderlich, C. Felser, The multiple directions of antiferromagnetic spintronics, Nat. Phys. 14 (2018) 200.
[17] I. Gavrikov, M. Seredina, M. Zheleznyy, I. Shchetinin, D. Karpenkov, A. Bogach, R. Chatterjee, V. Khovaylo, Magnetic and transport properties of Mn_2FeAl, J. Magn. Magn. Mater. 478 (2019) 55.
[18] J.V. Leitao, Y. Xinmin, L. Caron, E. Bruck, Magnetostructural study of the $(Mn,Fe)_3(P,Si)$ system, J. Alloy. Comp. 520 (2012) 52–58.
[19] H. Miki, K. Ohoyama, S. Funahashi, S. Tomiyoshi, Y. Yamaguchi, Crystallographic and magnetic structure of the itinerant-electron antiferromagnets $Mn_{3-x}T_xSi$ (T = Cr, Fe), Physica B 213-214 (1995) 360–362.
[20] S. Yoon, J.G. Booth, Magnetic properties and structures of some ordered $(FeMn)_3Si$ alloys, J. Phys. F Met. Phys. 7 (6) (1977) 1079.
[21] R. Kato, T. Nonoyama, R. Ooka, I. Shigeta, M. Hiroi, Transport properties of Heusler compounds $Fe_{3-x}Mn_xSi$ (x = 1.6, 1.7 and 1.8) under magnetic fields, AIP Adv. 8 (2018) 115019.
[22] T. Nonoyama, R. Kato, I. Shigeta, M. Hiroi, H. Manaka, N. Terada, Magnetic transition in the Heusler compounds $Fe_{3-x}Mn_xSi$, AIP Adv. 8 (2018) 115018.
[23] K. Buschow, P. van Engen, R. Jongebreur, Magneto-optical properties of metallic ferromagnetic materials, J. Magn. Magn. Mater. 38 (1983) 1.
[24] J. Kroder, J. Gooth, W. Schnelle, G.H. Fecher, C. Felser, Observation of spin glass behavior in chiral $Mn_{48}Fe_{34}Si_{18}$ with a β-Mn related structure, AIP Adv. 9 (2019), 055327.
[25] H.Z. Luo, H.W. Zhang, Z.Y. Zhu, L. Ma, S.F. Xu, G.H. Wu, X.X. Zhu, C.B. Jiang, H.B. Xu, Half-metallic properties for the Mn_2FeZ (Z=Al, Ga, Si, Ge, Sb) Heusler alloys: a first-principles study, J. Appl. Phys. 103 (2008), 083908.
[26] JuanRodríguez-Carvajal, Recent advances in magnetic structure determination by neutron powder diffraction, Phys. B Condens. Matter 192 (1993) 55.
[27] P. Blaha, K. Schwarz, G. Madsen, D. Kvasnicka, J. Luitz, WIEN2k: an Augmented Plane Wave Plus Local Orbitals Program for Calculating Crystal Properties, Vienna University of Technology, Austria, 2001.
[28] J. Balluff, Antiferromagnetic Heusler Compounds for Spintronics, Ph.D. thesis, Bielefeld University, Department of Physics, 2017.
[29] A. Jakobsson, P. Mavropoulos, E. Sasioglu, S. Blugel, M. Lezaic, B. Sanyal, I. Galanakis, First-principles calculations of exchange interactions, spin waves, and temperature dependence of magnetization in inverse-Heusler-based spin gapless semiconductors, Phys. Rev. B. 91 (2015) 174439.
[30] S. Skaftouros, K. Ozdogan, E. Sasioglu, I. Galanakis, Generalized Slater-Pauling rule for the inverse Heusler compounds, Phys. Rev. B. 87 (2013), 024420.
[31] S. Skaftouros, K. Ozdogan, E. Sasioglu, I. Galanakis, Search for spin gapless semiconductors: the case of inverse Heusler compounds, Appl. Phys. Lett. 102 (2013), 022402.
[32] Y. Xie, J. Ma, H. Vakilitaleghani, Y. Tan, A.W. Ghosh, Computational Search for ultrasmall and fast skyrmions in the inverse heusler family. 1901.09446.
[33] K. Hayashi, Y. Matsumura, S. Kobayashi, H. Morishita1, H. Koike, S. Miwa, N. Mizuochi, Y. Suzuki, Electron paramagnetic resonance study of MgO thin-film grown on silicon, J. Appl. Phys. 121 (2017) 213901.
[34] O. Gunnarsson, M. Calandra, J.E. Han, Colloquium: saturation of electrical resistivity, Rev. Mod. Phys. 75 (2003) 1085.
[35] E. Gratz, M.J. Zuckermann, Transport properties of rare earth intermetallic compounds (electrical resistivity, thermopower and thermal conductivity), J. Magn. Magn. Mater. 29 (1982) 181.
[36] J.K. Glasbrenner, B.S. Pujari, K.D. Belashchenko, Deviations from Matthiessen's rule and resistivity saturation effects in Gd and Fe from first principles, J. Magn. Magn. Mater. 89 (2014) 174408.